GaSb-Based Solar Cells for Full Solar Spectrum Energy Harvesting

Matthew P. Lumb, Shawn Mack, Kenneth J. Schmieder, María González, Mitchell F. Bennett, David Scheiman, Matthew Meitl, Brent Fisher, Scott Burroughs, Kyu-Tae Lee, John A. Rogers, and Robert J. Walters*

In this work, a multijunction solar cell is developed on a GaSb substrate that can efficiently convert the long-wavelength photons typically lost in a multijunction solar cell into electricity. A combination of modeling and experimental device development is used to optimize the performance of a dual junction GaSb/InGaAsSb concentrator solar cell. Using transfer printing, a commercially available GaAs-based triple junction cell is stacked mechanically with the GaSb-based materials to create a four-terminal, five junction cell with a spectral response range covering the region containing >99% of the available direct-beam power from the Sun reaching the surface of the Earth. The cell is assembled in a mini-module with a geometric concentration ratio of 744 suns on a two-axis tracking system and demonstrated a combined module efficiency of 41.2%, measured outdoors in Durham, NC. Taking into account the measured transmission of the optics gives an implied cell efficiency of 44.5%.

1. Introduction

To date, the most efficient device to convert solar photons to electrical power is a multijunction solar cell (MJSC).[1] This is a monolithic stack of solar cells which splits the solar spectrum into distinct spectral bands, thereby reducing the thermalization loss incurred by absorbing high energy photons in low bandgap semiconductors. Of the available materials for fabricating MJSCs, III–V semiconductors are unequalled in demonstrated conversion efficiency. Devices comprising these alloys (and, in some cases, the group IV element, germanium) have held the world record for conversion efficiency under concentrated sunlight for more than the last thirty years with steady increases in efficiency year-on-year.[2] Efficiency improvements result from many aspects of MJSC design, but among the most important of these are improving the distribution of light between the subcells of the MJSC, increasing the number of subcells, and increasing the fraction of the solar spectrum being captured.

The ideal MJSC would harvest the entire solar spectrum extending into the mid-infrared wavelength range using a very large number of closely spaced bandgaps, and the theoretical upper-limit of conversion efficiency is ≈86%, assuming full solar concentration of 45900 suns.[3] The Earth's atmosphere filters the solar spectrum, such that ≈99% of the power contained in the direct-beam airmass 1.5 (AM1.5D) reference spectrum is contained within the spectral band covering 300–2500 nm. This filtering impacts the optimal bandgaps for MJSCs, and recent calculations showed that the optimum lowest energy bandgap for practical MJSC solutions with 4–7 junctions is ≈0.5 eV (2500 nm).[4] These calculations assume more realistic device performance than the idealized, detailed-balance models,[5] and a more practical solar concentration of 1000X, which yields an efficiency projection of 54.6% for a 7 junction (7J) device. Therefore, to achieve virtually full spectrum energy harvesting of the direct-beam component of the terrestrial spectrum, 0.5 eV is the best practical target for the lowest bandgap absorber in an advanced MJSCs with four or more junctions. It should be noted that concentrator photovoltaic (CPV) solutions are typically unable to capture the diffuse portion of the irradiation, which can be a significant fraction of the global irradiation in terrestrial applications. However, recent advancements in hybrid approaches which combine CPV cells with larger area solar cells on the module back-plane to capture diffuse light[6] offer a potential route to even higher efficiency with respect to the total global irradiation incident on a photovoltaic module.

No single III–V or group IV substrate offers direct-bandgap, lattice-matched (LM) III–V alloys which span the entire spectral range at favorable bandgap intervals for producing MJSCs

Dr. M. P. Lumb
The George Washington University
2121 Ist, NW, Washington DC 20052, USA
E-mail: matthew.lumb.ctr.uk@nrl.navy.mil

Dr. S. Mack, Dr. K. J. Schmieder, D. Scheiman, Dr. R. J. Walters
US Naval Research Laboratory
4555 Overlook Avenue, SW, Washington DC 20375, USA

Dr. M. González, M. F. Bennett
Sotera Defense Solutions
430 National Business Pkwy #100, Annapolis Junction, MD 20701, USA

Dr. M. Meitl, Dr. B. Fisher, S. Burroughs
Semprius Inc.
4915 Prospectus Dr., Durham, NC 27713, USA

Dr. K.-T. Lee, Prof. J. A. Rogers
University of Illinois Urbana-Champaign
Urbana, IL 61801, USA

DOI: 10.1002/aenm.201700345

that capture the entire solar spectrum. In conventional solar cells used for concentrator applications, the longest wavelength extent of the spectral response range typically extends to ≈1800 nm or shorter, and consequently a significant fraction of the available power from the Sun is transmitted through the cell and wasted. The state-of-the-art in MJSC research focuses on techniques to extend the available bandgap range. This is achieved using a variety of methods, including metamorphic epitaxy;[7] the use of interesting alloys such as dilute nitrides[8] and bismides;[9] bandgap engineering using low dimensional semiconductors;[10] and heterogeneous integration by wafer bonding,[11] mechanical stacking,[12] or transfer printing.[13] The family of semiconductor alloys which can be grown LM to GaSb provides direct bandgaps in the range 0.27 to ≈1.0 eV,[14] and has previously been investigated for single junction thermophotovoltaic (TPV) applications[15] due to the availability of narrow bandgaps. Work has also been carried out in MJSCs grown on GaSb by liquid-phase epitaxy for TPV applications.[16] In this paper, we describe the development of high-performance MJSCs grown by molecular beam epitaxy (MBE) on GaSb for CPV applications and the subsequent integration of these materials with solar cells grown on GaAs substrates. Using transfer printing to achieve heterogeneous integration, we describe a 5 junction (5J) stacked solar cell that harvests almost the entire direct-beam solar spectrum using only high-quality, LM absorbers, resulting in ultrahigh conversion efficiency.

2. Bandgap Optimization

A convenient approach for exploring the optimum bandgaps for MJSCs is a detailed balance (DB) model. This model considers the limiting case where the only loss mechanism is through radiative recombination, and therefore over-estimates the conversion efficiency attained in practical scenarios. However, this simplistic model has some advantages. The model does not depend on specific material choices and doping for absorber and passivation layers, which if incorrectly chosen can have a negative impact on the predicted cell performance and therefore not reflect the practical limit. In addition, in previous work[17] we showed that, with a few simple modifications, the DB model may be adapted to produce efficiency predictions which are more representative of the practical upper limit in solar cell performance, while retaining the flexibility of the conventional DB model. The additional empirical loss factors introduced into the model include: less than unity absorbance of the subcells to account for their finite thickness, collection losses in the external quantum efficiency (EQE) to account for reflectivity and transport losses, an empirical open-circuit voltage loss over the DB prediction (V_{loss}) and series resistance loss. Therefore, bandgap combinations from this simple and flexible approach can then be used to inform cell designs in a more sophisticated charge-transport model capable of making quantitative predictions, to attempt to get as close to the practical upper limit as possible.

Figure 1a shows the predicted performance of a GaAs-based 3 junction (3J) + GaSb-based 2 junction (2J) mechanically stacked cell with different top and bottom cell bandgaps for the GaSb-based solar cell under 1000X AM1.5D illumination and at a cell temperature of 300 K. In this optimization, the GaAs-based part of the stack is unchanged and represents an InGaP/GaAs/InGaAsNSb 3J,[18] which is calculated to have a conversion efficiency of ≈43.2% at 1000X. The bandgaps and simulation details are summarized in Table S1 of the Supporting Information. The collection loss in the GaSb-based 2J was assumed to be greater than the GaAs 3J due to the combined effects of any optical loss at the mechanical interface and losses from the antireflection coating (ARC) on the GaAs 3J. The peak efficiency of the four-terminal cell is 47.37% with the efficiency of GaSb-based portion of the cell being 4.14%. This four terminal result assumes that the power outputs from each separate part of the mechanical stack are added together at their respective maximum power points and requires no current or voltage matching of the GaAs-based and GaSb-based parts of the stack. At first glance, this assumption may appear impractical from a module cost perspective due to the additional complexity of a four-terminal output. However, for a large array of cells, as in a CPV module, it has been shown that separate strings of GaAs-based and GaSb-based cells with different numbers of cells in series and parallel may be interconnected to make an overall current or voltage matched, two-terminal output.[19]

The optimal bandgaps are 0.75 eV and 0.51 eV for the GaSb-based top and bottom cells, respectively. The lattice matched quaternary alloy $In_{0.2}Ga_{0.8}As_{0.18}Sb_{0.82}$ is suitable to achieve a 0.51 eV bandgap absorber. A bandgap of 0.75 eV can be achieved using $Al_{0.015}Ga_{0.985}Sb$, but, from an engineering perspective, using bulk GaSb is advantageous to avoid the need for compositional calibration during growth. Furthermore, GaSb is likely to have fewer defects, longer minority carrier lifetimes and is less likely to degrade due to oxygen contamination than Al-containing alloys. The absorbance of the top cell in Figure 1a is assumed to be 96%, and by reducing this to 79%, a greater amount of photons is transmitted to the bottom cell for a given top cell bandgap, shifting the optimum top cell bandgap to 0.72 eV, as shown in Figure 1b. This modification has a small impact on the efficiency; there is minor penalty in voltage associated with the lower bandgap, which is partially offset by the additional photocurrent availability in both subcells, but overall the efficiency drops to 3.99% for the 2J and 47.22% for the 5J cell. This is shown in the LIV curves in Figure 1c for the optimum bandgap combinations with 96% and 79% GaSb-based top cell transparency, respectively. The LIV curve of the GaAs-based 3J is also shown. The EQE curves for the optimal 5J device with a GaSb/InGaAsSb 2J cell is shown in Figure 1d, along with the AM1.5D spectrum normalized to 1 kW m^{-2}. The 47.2% efficiency projection is intended to serve as a practical upper limit for this bandgap combination, lower than 51.7% in the case of a 5J with unconstrained bandgaps.[4] However, constraining our design to the use of currently commercially available technology for the GaAs-based part of the cell creates an opportunity for realizing a full spectrum energy harvesting solar cell commercially, and paves the way for even higher efficiency demonstrations using improved bandgap combinations in the future.

3. Cell Development

The following sections address the modeling, growth, and characterization of the components of the GaSb-based 2J solar

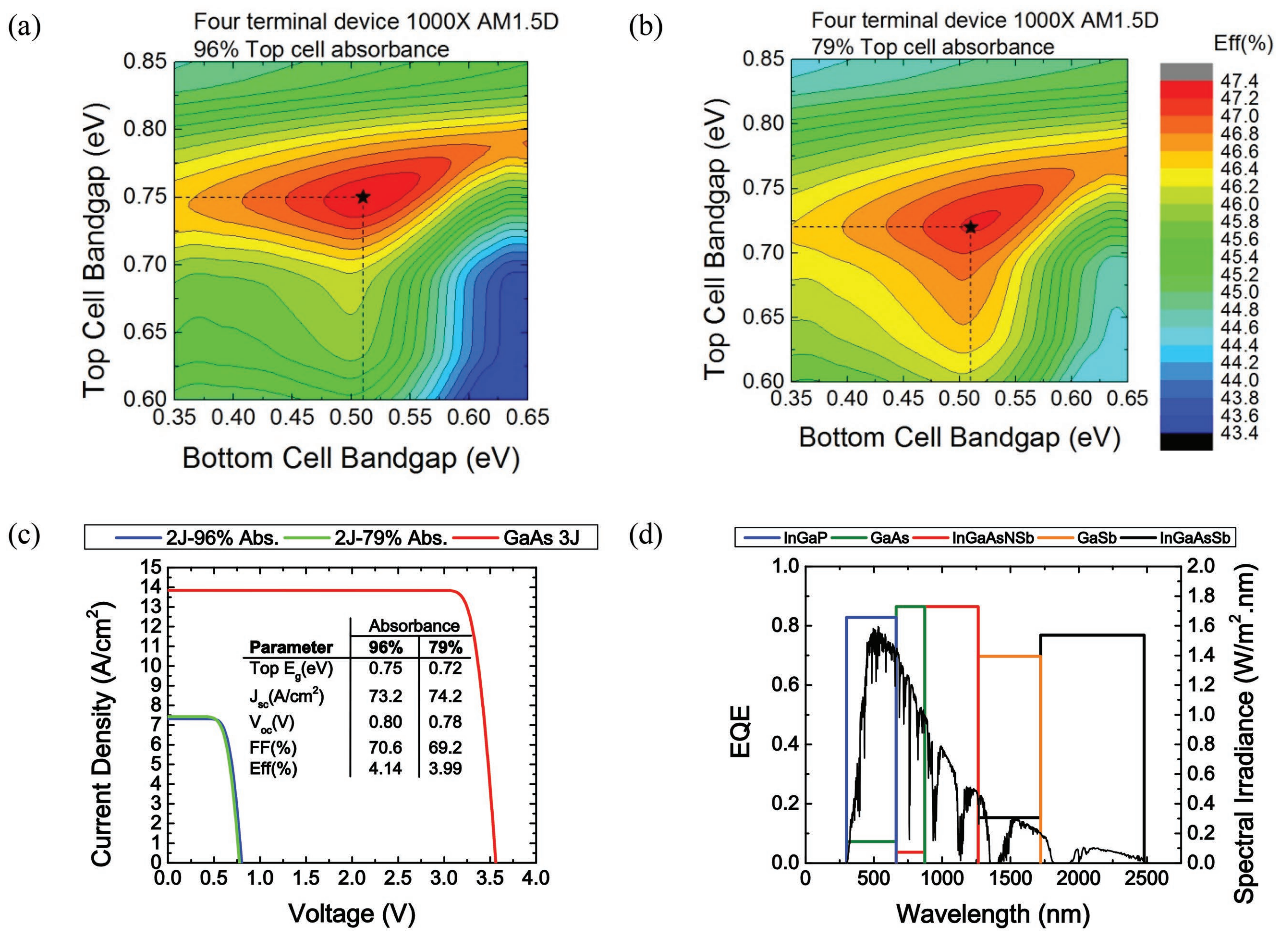

Figure 1. Modeled performance characteristics for mechanically stacked 5J solar cells. a) Calculated four terminal efficiency for as a function of GaSb-based 2J absorber bandgaps with a top cell absorbance of 96% and b) a top cell absorbance of 79%. c) Calculated LIV curves for the GaAs-based 3J and the optimum bandgap GaSb-based 2Js with top cell absorbance of 96% and 79%, respectively. d) External quantum efficiency ranges for the 5J alongside the AM1.5D spectrum showing complete spectral utilization out to 2500 nm.

cell, working toward the final demonstration of a mechanically stacked 5J cell capturing the entire solar spectrum.

3.1. Lateral Conduction Layer Development

The lateral conduction layer (LCL) is the topmost layer of the GaSb-based solar cell and designed to facilitate current spreading between the metal grid fingers of the cell. It is required to transmit photons of energy below ≈1 eV to the GaSb-based cells and achieve a low sheet resistance to minimize ohmic losses under high concentration conditions. The LCL employed here uses highly p-type $Al_{0.2}Ga_{0.8}Sb$ which is a good candidate material as it is closely lattice-matched to GaSb and has the desired direct bandgap.

As will be described in following sections, the solar cells in this paper have an n-on-p geometry. Therefore, typically a thick, wide-bandgap n-type layer would be appropriate for use as the front LCL. However, our design uses a highly p-type LCL layer because, as with Te-doped GaSb,[20] Hall measurements of n-type $Al_{0.2}Ga_{0.8}Sb$ grown by MBE revealed that the electrically active donor concentration using Te was limited to roughly 1×10^{18} cm^{-3}, hampering conductivity for n-type material. Furthermore, the majority carrier mobility of Te-doped $Al_{0.2}Ga_{0.8}Sb$ is reduced by roughly an order of magnitude relative to GaSb at comparable doping concentrations, shown in **Figure 2**a. In bulk GaSb, the presence of electrons in both the L and Γ conduction band valleys at temperatures above about 150 K has a non-negligible impact on the carrier mobility.[21] The smaller energy separation of the L and Γ conduction band valleys in $Al_{0.2}Ga_{0.8}Sb$ is therefore expected to result in a greater fraction of majority carriers residing in the lower mobility L-valley. Greater inter-valley scattering in $Al_{0.2}Ga_{0.8}Sb$ than GaSb[21] may also play a significant role in reducing the electron mobility. In fact, the experimental majority carrier mobility of n-type $Al_{0.2}Ga_{0.8}Sb$ is close to that of p-type $Al_{0.2}Ga_{0.8}Sb$ at similar doping levels. However, the electrically active concentration can be much greater in p-type $Al_{0.2}Ga_{0.8}Sb$, enabling more than an order of magnitude reduction in resistivity, shown in Figure 2b. Therefore, p-type $Al_{0.2}Ga_{0.8}Sb$ is advantageous for the LCL, but the choice of n-on-p geometry for the solar cells requires a tunnel junction to be placed between the LCL and the cell.

The tunnel junctions used throughout this work are broken-gap quantum-well tunnel junctions, which use a thin,

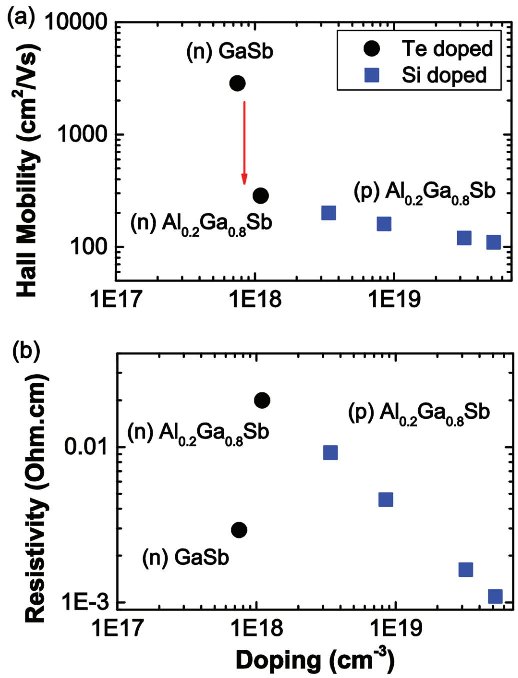

Figure 2. a) Measured Hall mobility and b) resistivity for Te and Si doped GaSb and AlGaSb with different electrically active dopant concentrations.

heterostructure quantum well at the n/p interface of the tunnel device. The quantum well has a type-III, or broken-gap alignment to the surrounding bulk layers and provides an extremely low resistance barrier for tunneling between the conduction band and valence band whilst maintaining a high transparency. A detailed discussion of the design and properties of these devices can be found in reference [22].

3.2. GaSb and InGaAsSb 1J Development

Single junction (1J) GaSb and InGaAsSb cells, designed using NRL MultiBands, were grown by MBE and fabricated into solar cells. The model uses an analytical drift-diffusion approach with accurate optical constants, carrier transport and band parameters, and also includes coherent optical effects due to interface reflections and photon recycling.[23] The charge transport in the model is one-dimensional and interfaces in the model are treated as abrupt and smooth. The transfer matrix method is used to calculate the reflectivity of multilayered media, using a mixture of literature values for optical constants, with interpolation between existing composition points where necessary, and optical constants derived from ellipsometric measurements on test films. The 1J devices serve as useful structures for optimizing the design of the components of the final 2J cell and for calibrating the drift-diffusion model inputs. Initial diode test structures of GaSb and InGaAsSb homojunctions revealed that lower dark current was attained in the n-on-p geometry and therefore both single junction devices were grown in an n-on-p configuration.

The EQE of the GaSb 1J solar cell is shown in **Figure 3**a. Excellent agreement with the NRL MultiBands model was achieved by adjusting the surface recombination velocity (SRV) and Shockley Read Hall lifetime for minority carriers in the emitter and base, until good agreement with both EQE and dark current–voltage (DIV) was achieved. The extracted values for SRV and minority carrier diffusion length, along with the complete layer structures, are summarized in Table S2 of the Supporting Information. The internal quantum efficiency (IQE), defined as $IQE = EQE/(1 - R)$, where R is the reflectivity at normal incidence, was found to have a peak value of 91.6%, demonstrating the high performance of the MBE grown material. This GaSb solar cell test structure did not have a thick

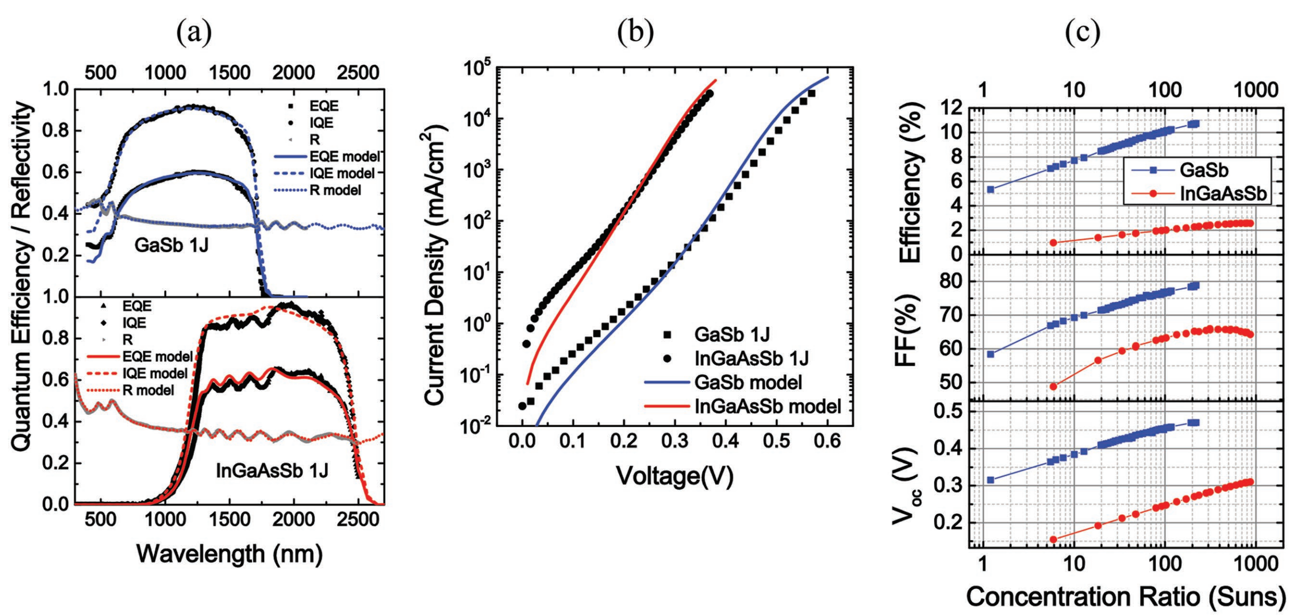

Figure 3. a) Measured (points) and modeled (lines) reflectivity, external quantum efficiency, and internal quantum efficiency for GaSb and InGaAsSb single junction solar cells. b) Measured (points) and modeled (lines) dark current density for GaSb and InGaAsSb solar cells. c) Measured LIV figures of merit for the GaSb and InGaAsSb solar cells, with the concentration ratio determined from implied 1 sun photocurrent values extracted from EQE.

p-type LCL, but rather a thin n-type $Al_{0.2}Ga_{0.8}Sb$ window layer to improve light transmission to the cell and a thin (10 nm) n-type InAs cap to achieve ohmic contact. The InAs cap layer has a small impact on the quantum efficiency, creating parasitic absorption, which is taken into account in the model. The close agreement of the measured reflectivity with the modeled data is evident in Figure 3a. However, the modeled layer thicknesses were adjusted slightly from their nominal design values to improve the quality of the fit, which is reasonable considering small uncertainties in growth rate and across-wafer deviations.

Figure 3a also shows the EQE and IQE for the InGaAsSb 1J solar cell, with the structure given in Table S3 of the Supporting Information. This cell includes a thick, p-type $Al_{0.2}Ga_{0.8}Sb$ lateral conduction layer which filters the short wavelength photons and a broken-gap quantum well tunnel junction. Excellent agreement with NRL MultiBands was also achieved for this structure, and the extracted SRV and diffusion length values are summarized in Table S3 of the Supporting Information. The maximum IQE for this cell was 96.9%, and excellent agreement was also found with the measured reflectivity. The DIV curves for both samples, measured using a four point probe technique on 1 mm diameter, fully metallized circular mesas is shown in Figure 3b. Good agreement is demonstrated in forward bias with the model, but both devices showed increased dark current at low biases, which is attributed to leakage current through the sidewalls of the device.

Laboratory LIV measurements of the GaSb and InGaAsSb solar cells at concentration were conducted and Figure 3c shows the efficiency, fill factor, and open-circuit voltage of each cell measured as a function of concentration, assuming photocurrent levels equivalent to illumination from the ASTM AM1.5D spectrum normalized to 1 kW m^{-2}. The experimental details are given in the Experimental Section. Neither cell had an ARC which significantly reduces the efficiency values observed. However, the FF and V_{oc} of each device demonstrate that high material quality was achieved for both cells and that both are able to operate at high concentration without incurring significant fill factor losses due to series resistance.

4. Full Spectrum Energy Harvesting Demonstration

Using the information gathered from device results for the single junction solar cells, a dual junction solar cell was designed and grown. The layer structure is given in Table S4 of the Supporting Information, and the top cell base thickness was thinned to ensure current matched performance in a mechanically stacked architecture, with the optimum thickness calculated using the analytical drift-diffusion model. The necessity to thin the GaSb based cell also follows from the DB model predictions in Figure 1, demonstrating good agreement between the far less comprehensive DB approach with a model using real optical constants and material properties. The simulated EQE and IQE for the 2J cell are shown in **Figure 4**a, prior to stacking with the commercial GaAs-based 3J. The actual cell exhibited high leakage current at the low current levels associated with EQE measurements, preventing reliable EQE measurements to be taken for comparison to the model predictions. Light-biasing was attempted to reduce the impact of the leakage current, but the light-biasing intensity levels attained were insufficient to enable reliable EQE measurements to be made. However, as will be discussed in the following section, the photocurrent production of the cell ascertained from outdoor measurements matched well with model predictions. The measured reflectivity of the cell was in close agreement with the modeled data, also shown in Figure 4a. The estimated short-circuit current density of the GaSb top cell and InGaAsSb bottom cell under the ASTM AM1.5D spectrum, normalized to 1 kW m^{-2}, are 7.26 and 6.31 mA cm^{-2}, respectively.

4.1. Mechanical Stacking

Transfer printing[24] was used to achieve heterogeneous integration of the GaAs-based cell with the GaSb-based cell. The commercial GaAs 3J cell was grown on top of an AlInP release layer then processed by Semprius Inc. and subsequently printed using the procedure described in references[19a] and[17]. The rear contact of the GaAs cell was formed using a front facing contact

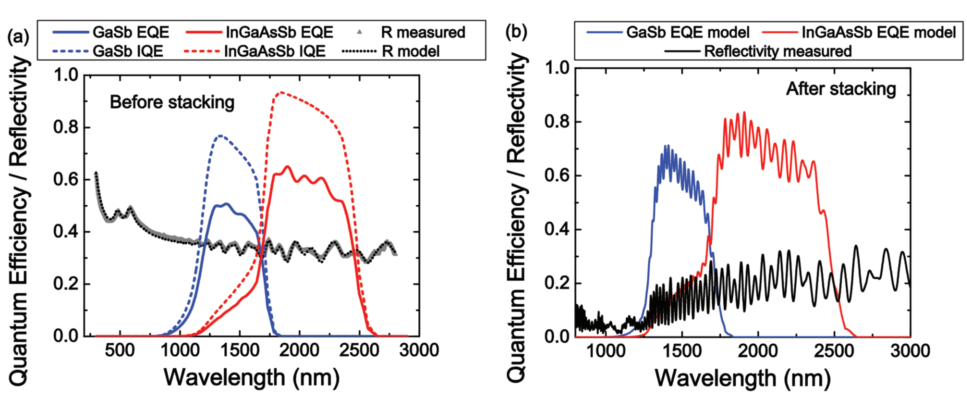

Figure 4. a) Calculated external and internal quantum efficiency for the GaSb/InGaAsSb 2J solar cell. The quantum efficiency curves are calculated using the analytical drift-diffusion model with calibration data from fitting results for single junction devices. The measured and modeled reflectivity for the device is also shown. b) The measured reflectivity and calculated external and internal quantum efficiency for the GaSb/InGaAsSb 2J solar cell after stacking with a GaAs 3J. The EQE curves were computed using the experimentally measured reflectivity for stacked device, and corrected for the simulated transmission through the GaAs 3J.

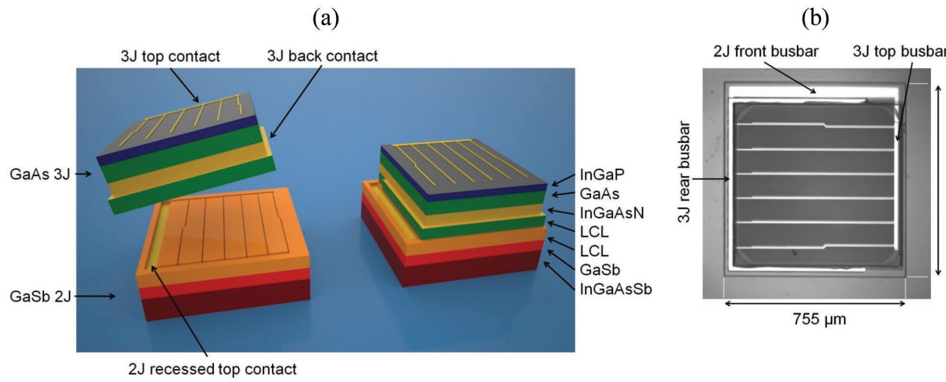

Figure 5. a) Schematic representation of the heterogeneous integration of the GaAs-based 3J cell and the GaSb-based 2J cell. b) NIR microscope image of a GaAs 3J stacked on a GaSb 2J device.

to a highly doped GaAs LCL. A thin (<20 nm) polymeric adhesive layer was spin coated upon the surface of the GaSb cell to promote void-free bonding between the devices.

The top contact of the GaSb-based 2J was embedded into the AlGaSb LCL by a depth of 1 µm to ensure a planar surface for printing. Figure 4b shows the measured reflectivity and calculated EQE for the GaSb 2J after stacking with the GaAs 3J. The EQE curves were approximated by multiplying the internal quantum efficiency for each device, shown in Figure 4a, by the transmission of the GaAs 3J solar cell, ascertained from the measured reflectivity and the absorption in the bottom cell of the 3J. The EQE after stacking increases in comparison to the unstacked devices due to the reduction in overall reflectivity, owing to the three layer ARC on the GaAs cell. However, the increased filtering to the GaSb cell due to absorption in the GaAs 3J results in an overall reduction in photocurrent in that cell. The estimated short-circuit current density of the GaSb top cell and InGaAsSb bottom cell under the ASTM AM1.5D spectrum, normalized to 1 kW m^2, are 5.64 and 7.29 mA cm^{-2}, respectively. A schematic of the mechanically stacked device is shown in **Figure 5**a, labeling the key components of each cell. The GaSb-based cells remained attached to their native substrate for the purposes of this experiment, and the back contact for these cells was applied to the rear side of the substrate.

The transfer printing technique enables placement precision of printed chiplets to dimensions on the order of 1 micron. A typical example of a well-aligned, mechanically stacked cell comprising the GaAs-3J and GaSb-2J is shown in Figure 5b. This image is captured using a near infrared microscope, which images using wavelengths transmitted by the GaAs-based cell, allowing an image of the bond interface and metallization features on the GaSb-based cell to be observed. The absence of voids and precise overlap of grid fingers on the two cells is clearly visible.

4.2. Outdoor Measurements

Evaluating the efficiency of the mechanically stacked cell under ASTM AM1.5D conditions using a calibrated solar simulator is problematic due to the absence of calibrated broadband sources over the full range of wavelengths from 300 to 2500 nm. However, by building a mini-module, the cell may be tested outdoors to gain valuable information about the cell performance and facilitate the use of modeling to extrapolate the cell performance to AM1.5D conditions.

To test the microcell, a portable probe stage with integrated concentrator lens was assembled and mounted on a two axis tracking system, based in Durham, NC. To concentrate the sunlight on the cell, a 25 mm diameter spherical, achromatic lens was chosen, which maintains a tight circular focal spot within the aperture area of the cell over the whole spectral range. Outdoor measurements were taken on the afternoon of the 5th of October 2016. The direct normal irradiance (DNI) and global normal irradiance during the measurements were monitored using an Eppley normal incidence pyroheliometer and an Eppley pyranometer, respectively. The transmission of the lens was characterized using a spectrophotometer and integrating sphere and is shown in **Figure 6**. The lens demonstrated transmission exceeding 75% over the whole spectral response range of the 5J, although the IR wavelengths are attenuated due to absorption in the glass. Based upon the location and time of day, the airmass of the direct beam spectrum was determined to be very close to 2. Therefore, to estimate the spectral irradiance of light on the cell after transmission through the lens

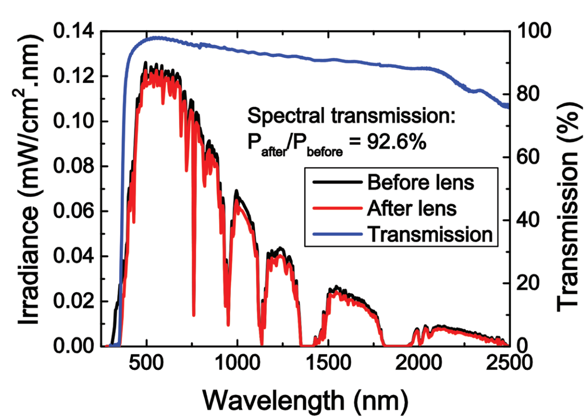

Figure 6. Transmission function of the achromatic doublet lens measured using a spectrophotometer and integrating sphere setup. The modeled AM2 spectrum before and after the lens is also shown, resulting in a total power transmission of 92.6% through the lens.

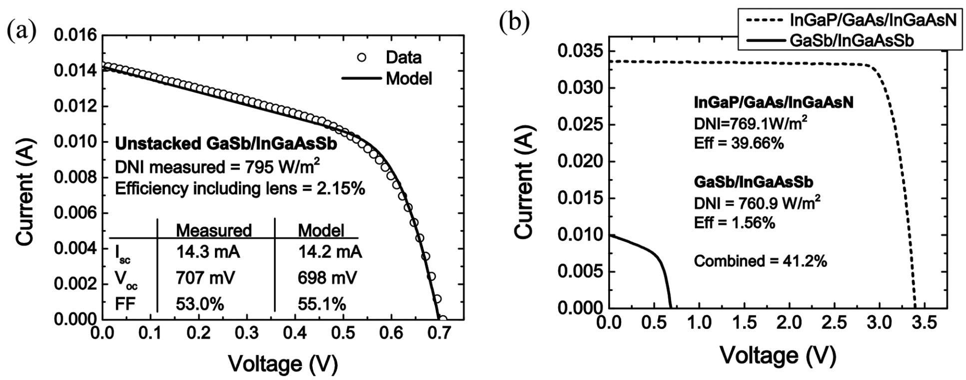

Figure 7. Outdoor measurements of stacked and unstacked solar cells. a) Measured and modeled LIV curve for the unstacked GaSb/InGaAsSb 2J cell measured outdoors under concentrated sunlight. b) Measured LIV for the GaAs 3J and GaSb 2J mini-module measured outdoors under concentrated sunlight.

at any given moment, the AM2 spectrum, normalized to the measured DNI, was multiplied by the measured lens transmission. The total fraction of integrated intensity of the AM2 spectrum transmitted through the lens was found to be 92.6%.

Figure 7a shows LIV measurements for an unstacked GaSb/InGaAsSb 2J, and the model prediction is also shown as the solid line. The I_{sc} and V_{oc} are in excellent agreement using the modeled device performance, but a significant shunt contribution was required in order to reproduce the shape of the LIV curve. A shunt resistance of 0.85 Ω cm^2 and a series resistance of 1.8×10^{-2} Ω cm^2 was found to give good agreement to the measured LIV characteristics. The proposed explanation for the low shunt resistance is perimeter recombination at the exposed, unpassivated sidewalls, exacerbated by the small cell size in this demonstration, and is a well-known challenge with narrow-gap GaSb-based materials.[25] The exact nature of the leakage current is not known at this time, but the fully exposed sidewalls of the GaSb top cell during the 2J mesa isolation may have a significant role. The shunt resistance has a negative impact on the device efficiency primarily due to FF reduction: the predicted FF of the cell with an infinite shunt resistance under the illumination conditions in Figure 7a is 78.0%. Improving perimeter recombination through process development and sidewall passivation strategies promises to improve the efficiency still further.

The LIV curve of the 2J after stacking is shown in Figure 7b, and the efficiency of the 2J and lens combined is 1.56%. The GaAs 3J was measured within minutes of the GaSb 2J under very similar spectral conditions, and the efficiency of the 3J plus lens was found to be 39.66%, giving a combined four terminal efficiency of the mini-module of 41.22%. Based upon the estimated spectral power transmission through the lens of 92.6%, the efficiency of the GaSb-based 2J and GaAs-based 3J with respect to the light transmitted through the lens is estimated to be 1.7% and 42.8%, respectively, giving a combined four terminal efficiency of 44.5%. Note, this cell efficiency metric considers the spectrum incident upon the cell in our particular outdoor measurement, and is therefore not directly comparable to standard test conditions measured under airmass 1.5 illumination. The figures of merit for both components of the 5J cell are summarized in **Table 1**. The ARC on the GaAs 3J aids in the photon collection of light transmitted to the GaSb/InGaAsSb 2J cell, which has previously been shown to boost the performance of underlying cells in a mechanical stack over the unstacked value.[13] As shown in Figure 4b, in the stacked configuration, the increased filtering of light to the top cell from the GaAs 3J acts to reduce the GaSb cell photocurrent, but the increased light coupling into the GaSb cell due to the presence of an ARC increases the peak external quantum efficiency in both GaSb and InGaAsSb cells. In practice, the photocurrent produced by the GaSb-based cell after stacking was lower than the unstacked cell. This is in part due to the ARC applied to the GaAs-based 3J not being optimized for broadband transmission over the entire solar spectrum, and therefore insufficient to recover the reduction in photocurrent due to filtering. Also, some photons are lost due to reflection at the mechanical interface. The filtering of light to the GaSb-based cell is also increased if the GaAs-based cell is operating at an elevated temperature, as the redshift in the absorption edge of the lowermost GaAs-based cell filters more photons. To remedy these effects, however, the transmission of both the front surface ARC and the mechanical interface may be readily improved using better optimized dielectric film stacks to minimize unwanted reflections and, coupled with improved sidewall passivation of the GaSb-based cell, will increase the performance closer to the practical limiting efficiency of 47.2% for this bandgap configuration.

Table 1. Measured figures of merit for the stacked GaSb 2J and GaAs 3J under concentrated sunlight illumination.

Parameter	GaSb 2J	GaAs 3J
I_{sc} [mA]	9.98	33.62
V_{oc} [V]	0.688	3.398
FF [%]	54.2	83.9
Efficiency of mini-module [%]	1.56	39.66
Efficiency of cell [%]	1.7	42.7

5. Conclusions

The GaSb substrate offers lattice-matched, direct-bandgap materials which are able to efficiently convert IR photons to produce a mechanically stacked solar cell which covers the spectral range supplying >99% of the available power from the sun reaching the surface of the Earth. In this work, a 2J solar cell grown on GaSb by MBE has been developed and characterized. Key aspects of cell design, LCL development and material choices have been analyzed using a combination of modeling and experimental investigation. Using transfer printing, a four-terminal, mechanically stacked 5J solar cell was produced and characterized in a mini-module with a geometric concentration ratio of 744 suns employing a spherical achromatic doublet lens and two-axis tracking. Outdoor measurements in Durham, NC, were used to characterize the mini-module, which demonstrated 41.2% efficiency, and an estimated cell efficiency of 44.5% was implied based upon the transmission of the optics and the typical spectral content for the location and time of the measurements. Optimization of photovoltaics capturing photons with wavelengths extending to 2500 nm is a key development stage on the route to practical concentrator MJSCs which can achieve cell efficiencies in excess of 54%.

6. Experimental Section

Device Fabrication: Both GaSb single junction, InGaAsSb single junction, and GaSb/InGaAsSb dual junction solar cells were fabricated in this work using the same procedure. For devices not designed for mechanical stacking, unannealed Ti/Pt/Au front side contacts were defined using standard photolithographical procedures. In devices designed to be suitable for mechanical stacking, recessed front-side contacts were fabricated in the AlGaSb LCL using an inductively coupled plasma reactive ion etching procedure. In this case, standard photolithographic techniques were used to define trenches in an SiN_x hard mask. Dry etching was then carried out using a BCl_3/Ar chemistry, which allowed for controlled etch rates to produce smooth etched surfaces with anisotropic profiles.[26] Unannealed Ti/Pt/Au contacts were deposited in the etched trenches using a standard liftoff process and device isolation was performed using a phosphoric-based mesa wet etch chemistry. In all cases, the rear-side contact was formed using unannealed Ti/Au deposited on the back side of the substrate.

Device Testing: All the electrical measurements for the devices in this paper were performed using a standard four-point probe technique and a Keithley 2401 Sourcemeter. *I–V* curves were measured using forward sweeps with 100 ms intervals between measurement points. EQE measurements were performed on the cells using Xe lamp spectrum dispersed using a monochromator and modulated by a chopper wheel at 17 Hz. The incident power was determined over the whole spectral range using a calibrated pyrometer. No voltage bias was applied to the cells during the measurements, but a white light bias was applied using a halogen lamp.

The GaSb solar cell shown in Figure 3 was mounted on a temperature controlled vacuum chuck set to a temperature of 25 °C and illuminated using an Oriel solar simulator with an AM1.5D filter and with a 75 mm diameter Thorlabs LA1002 plano-convex lens. The aperture area of the cell was 0.995 mm^2 and the concentration ratio was determined from the 1 sun short-circuit current, established from the EQE measurements, adjusted for the shading from the grid pattern, and using the ASTM AM1.5D reference spectrum normalized to 1 kW m^{-2}. The irradiance power was assumed to be linearly proportional to the measured I_{sc} of the solar cell. Different concentration values were achieved by defocusing the spot from the lens using an adjustable height stage.

For the InGaAsSb solar cell shown in Figure 3, insufficient power was available from the Oriel solar simulator to achieve high concentration with this cell, so it was characterized using illumination from a 1345 nm laser with variable power. The aperture area of this cell was 0.4225 mm^2 and, as with the GaSb cell, the concentration ratio was determined from the 1 sun I_{sc} value established from EQE measurement assuming the ASTM AM1.5D reference spectrum normalized to 1 kW m^{-2}.

The specular reflectance of the devices shown in Figure 4a was measured with a LAMBDA 750 UV/Vis/NIR Spectrophotometer, made by PerkinElmer Inc. A calibrated Al mirror was used to measure absolute reflectance. The specular reflectance of the mechanically stacked device in Figure 4b was measured using a Bruker 80v spectrometer that is coupled to an all-reflective, infrared microscope (Bruker Hyperion 1000). The microscope was fit with all-reflective optics, including a reverse-Cassegrain microscope objective that focused unpolarized infrared light onto the sample and collected light reflected by the sample (angle of incidence and collection angle varied from 22°–23.6°). The reflected light was focused onto and detected by an InSb/MCT sandwich detector.

Outdoor Measurements: A custom built probe stage was assembled to test probe the mechanically stacked cells. Figure S1 of the Supporting Information showed the features of the stage, which included a water-cooled copper vacuum chuck with *xy* motion and a lens mount with *xyz* motion. The temperature of the chuck was set to be 25 °C. Rear contact to the GaSb-based cell was achieved through the vacuum chuck, and six needle point probes mounted on mechanical manipulators were used to complete four point probe connections to the individual GaAs and GaSb-based cells. The whole stage was then mounted on a two-axis tracking system in Durham, NC.

To concentrate the sunlight on the cell, a 25 mm diameter Newport PAC040 spherical achromatic lens was chosen, which maintained a tight focal spot within the aperture area of the cell (650 µm × 650 µm) over the whole spectral range, which was verified using ray tracing simulations. The lens was mounted in a holder with a 20 mm diameter circular aperture giving a total power-in area of 3.142 cm^2. Relative to the aperture area of the cell of 0.4225 mm^2, this gave a geometric concentration ratio of 744 suns. No secondary optic was used.

An Eppley normal incidence pyroheliometer was also mounted on the tracker to monitor the direct-beam irradiance throughout the tests. The total power-in of direct-beam illumination incident on the mini-module, used for efficiency determination, was calculated using the output of the pyroheliometer multiplied by the aperture area of the focusing lens holder of 3.142 cm^2.

Supporting Information

Supporting Information is available from the Wiley Online Library or from the author.

Acknowledgements

The authors would like to thank Dr. Michael K. Yakes, Dr. Behrang Hamadani, Dr. Chase Ellis, and Dr. Joseph Tischler for helpful contributions to this work. This work was supported by the Office of Naval Research and in part by ARPA-E MOSAIC program number 1255–1544, "Micro-scale, Ultra-high Efficiency CPV/Diffuse Hybrid Arrays Using Transfer Printing".

Conflict of Interest

The authors declare no conflict of interest.

Keywords

GaSb, multijunction, solar cells, transfer-printing

Received: February 8, 2017
Revised: April 28, 2017
Published online: July 10, 2017

[1] a) M. A. Green, K. Emery, Y. Hishikawa, W. Warta, E. D. Dunlop, D. H. Levi, A. W. Y. Ho-Baillie, *Prog. Photovoltaics* **2017**, *25*, 3; b) R. R. King, *Nat. Photonics* **2008**, *2*, 284; c) M. Steiner, G. Siefer, T. Schmidt, M. Wiesenfarth, F. Dimroth, A. W. Bett, *IEEE J. Photovoltaics* **2016**, *6*, 1020.
[2] NREL. *Research Cell Record Efficiency Chart*, http://www.nrel.gov/pv/assets/images/efficiency_chart.jpg (accessed: November 2016).
[3] A. De Vos, *J. Phys. D: Appl. Phys.* **1980**, *13*, 839.
[4] M. P. Lumb, M. Meitl, K. J. Schmieder, M. González, S. Mack, M. Yakes, M. F. Bennett, J. Frantz, M. A. Steiner, J. F. Geisz, D. J. Friedman, M. A. Slocum, S. M. Hubbard, B. Fisher, S. Burroughs, R. J. Walters, *presented at 43rd IEEE Photovoltaics Specialists Conf.*, Portland, OR, USA, June **2016**.
[5] G. Letay, A. W. Bett, *presented at 17th European Photovoltaic Energy Conf.*, Munich, Germany, October **2001**, p. 178.
[6] K.-T. Lee, Y. Yao, J. He, B. Fisher, X. Sheng, M. Lumb, L. Xu, M. A. Anderson, D. Scheiman, S. Han, Y. Kang, A. Gumus, R. R. Bahabry, J. W. Lee, U. Paik, N. D. Bronstein, A. P. Alivisatos, M. Meitl, S. Burroughs, M. M. Hussain, J. C. Lee, R. G. Nuzzo, J. A. Rogers, *Proc. Natl. Acad. Sci. USA* **2016**, *113*, E8210.
[7] a) J. F. Geisz, D. J. Friedman, J. S. Ward, A. Duda, W. J. Olavarria, T. E. Moriarty, J. T. Kiehl, M. J. Romero, A. G. Norman, K. M. Jones, *Appl. Phys. Lett.* **2008**, *93*, 123505; b) R. King, D. Law, K. Edmondson, C. Fetzer, G. Kinsey, H. Yoon, R. Sherif, N. Karam, *Appl. Phys. Lett.* **2007**, *90*, 183516.
[8] D. B. Jackrel, S. R. Bank, H. B. Yuen, M. A. Wistey, J. S. Harris Jr, A. J. Ptak, S. W. Johnston, D. J. Friedman, S. R. Kurtz, *J. Appl. Phys.* **2007**, *101*, 114916.
[9] T. Thomas, A. Mellor, N. Hylton, D. Alonso, A. Braun, N. Ekins-Daukes, J. David, S. Sweeney, *Semicond. Sci. Technol.* **2015**, *30*, 094010.
[10] N. Ekins-Daukes, K. Barnham, J. Connolly, J. Roberts, J. Clark, G. Hill, M. Mazzer, *Appl. Phys. Lett.* **1999**, *75*, 4195.
[11] F. Dimroth, M. Grave, P. Beutel, U. Fiedeler, C. Karcher, T. N. D. Tibbits, E. Oliva, G. Siefer, M. Schachtner, A. Wekkeli, A. W. Bett, R. Krause, M. Piccin, N. Blanc, C. Drazek, E. Guiot, B. Ghyselen, T. Salvetat, A. Tauzin, T. Signamarcheix, A. Dobrich, T. Hannappel, K. Schwarzburg, *Prog. Photovoltaics* **2014**, *22*, 277.
[12] M. A. Steiner, J. F. Geisz, J. S. Ward, I. García, D. J. Friedman, R. R. King, P. T. Chiu, R. M. France, A. Duda, W. J. Olavarria, M. Young, S. R. Kurtz, *IEEE J. Photovoltaics* **2016**, *6*, 358.
[13] M. P. Lumb, M. Meitl, B. Fisher, S. Burroughs, K. J. Schmieder, M. Gonzalez, M. K. Yakes, S. Mack, R. Hoheisel, M. F. Bennett, C. W. Ebert, D. V. Forbes, C. G. Bailey, R. J. Walters, *presented at 42nd IEEE Photovoltaic Specialist Conf.*, New Orleans, LA, USA, June **2015**, p. 1.
[14] I. Vurgaftman, J. R. Meyer, L. R. Ram-Mohan, *J. Appl. Phys.* **2001**, *89*, 5815.
[15] a) M. G. Mauk, V. M. Andreev, *Semicond. Sci. Technol.* **2003**, *18*, S191; b) A. Bett, O. Sulima, *Semicond. Sci. Technol.* **2003**, *18*, S184; c) Z. A. Shellenbarger, G. C. Taylor, R. K. Smeltzer, J. Li, R. U. Martinelli, K. Palit, *presented at Fifth Conf. Thermophotovoltaic Generation of Electricity*, Rome, Italy, September **2002**, p. 314; d) O. V. Sulima, A. W. Bett, *Sol. Energy Mater. Sol. Cells* **2001**, *66*, 533; e) C. A. Wang, H. K. Choi, D. C. Oakley, G. W. Charache, *presented at AIP Conf. Proc.*, Denver, CO, USA, October **1999**, p. 256; f) F. Dimroth, C. Agert, A. W. Bett, *J. Cryst. Growth* **2003**, *248*, 265.
[16] a) V. M. Andreev, V. P. Khvostikov, V. R. Larionov, V. D. Rumyantsev, S. V. Sorokina, M. Z. Shvarts, V. I. Vasil'ev, A. S. Vlasov, *presented at 26th IEEE Photovoltaic Specialists Conf.*, Anaheim, CA, USA, September **1997**, p. 935; b) V. M. Andreev, V. P. Khvostikov, V. D. Rumyantsev, S. V. Sorokina, M. Z. Shvarts, *presented at 28th IEEE Photovoltaic Specialists Conf.*, Anchorage, AK, USA, September **2000**, p. 1265.
[17] M. P. Lumb, M. Meitl, J. W. Wilson, S. Bonafede, S. Burroughs, D. V. Forbes, C. G. Bailey, N. M. Hoven, M. Gonzalez, M. K. Yakes, S. J. Polly, S. M. Hubbard, R. J. Walters, *presented at 40th IEEE Photovoltaics Specialists Conf.*, Denver, CO, USA, June **2014**.
[18] D. Derkacs, R. Jones-Albertus, F. Suarez, O. Fidaner, *J. Photonics Energy* **2012**, *2*, 021805.
[19] a) X. Sheng, C. A. Bower, S. Bonafede, J. W. Wilson, B. Fisher, M. Meitl, H. Yuen, S. Wang, L. Shen, A. R. Banks, C. J. Corcoran, R. G. Nuzzo, S. Burroughs, J. A. Rogers, *Nat. Mater.* **2014**, *13*, 593; b) M. P. Lumb, K. J. Schmieder, M. González, S. Mack, M. K. Yakes, M. Meitl, S. Burroughs, C. Ebert, M. F. Bennett, D. V. Forbes, X. Sheng, J. A. Rogers, R. J. Walters, *presented at CPV 11*, Aix Les Bains, France, April **2015**, p. 040007.
[20] a) A. Chandola, R. Pino, P. S. Dutta, *Semicond. Sci. Technol.* **2005**, *20*, 886; b) T. H. Chiu, J. A. Ditzenberger, H. S. Luftman, W. T. Tsang, N. T. Ha, *Appl. Phys. Lett.* **1990**, *56*, 1688; c) G. W. Turner, S. J. Eglash, A. J. Strauss, *J. Vac. Sci. Technol., B* **1993**, *11*, 864.
[21] V. W. L. Chin, *Solid-State Electron.* **1995**, *38*, 59.
[22] M. P. Lumb, S. Mack, M. González, K. J. Schmieder, R. J. Walters, *US20160211393 A1* **2016**.
[23] a) M. P. Lumb, C. G. Bailey, J. G. J. Adams, G. Hillier, F. Tuminello, V. C. Elarde, R. J. Walters, *IEEE J. Quantum Electron.* **2013**, *49*, 462; b) M. P. Lumb, M. A. Steiner, J. F. Geisz, R. J. Walters, *J. Appl. Phys.* **2014**, *116*, 194504.
[24] a) M. A. Meitl, Z.-T. Zhu, V. Kumar, K. J. Lee, X. Feng, Y. Y. Huang, I. Adesida, R. G. Nuzzo, J. A. Rogers, *Nat. Mater.* **2006**, *5*, 33; b) J. Kim, J. Hwang, K. Song, N. Kim, J. C. Shin, J. Lee, *Appl. Phys. Lett.* **2016**, *108*, 253101.
[25] H. Kim, E. Plis, A. Khoshakhlagh, S. Myers, N. Gautam, Y. Sharma, L. Dawson, S. Krishna, S. Lee, S. Noh, *Appl. Phys. Lett.* **2010**, *96*, 033502.
[26] M. F. Bennett, M. P. Lumb, M. González, K. J. Schmieder, S. Mack, J. A. Nolde, R. J. Walters, *presented at 43rd IEEE Photovoltaic Specialists Conf. (PVSC)*, Portland, OR, USA, June **2016**, p. 2323.